Journal of Magnetic Resonance **148,** 349–354 (2001)
doi:10.1006/jmre.2000.2240, available online at http://www.idealibrary.com on IDEAL®

One-Shot Velocimetry Using Echo Planar Imaging Microscopy

Song-I Han* and Paul T. Callaghan†

†*Institute of Fundamental Sciences—Physics, Massey University, Palmerston North, New Zealand; and* **Institute of Technical Chemistry and Macromolecular Chemistry, Rheinisch-Westfälische Technische Hochschule, 52056 Aachen, Germany*

Received July 12, 2000; revised October 3, 2000

A rapid version of PEPI (π-echo planar imaging) velocimetry has been implemented, enabling a velocity image, at microscopic resolution, to be acquired in less than 1 s. The velocity map was reconstructed using the phase information from the ratio of two PEPI images, one obtained with a velocity-encoding filter applied prior to the imaging sequence and the other image without. The acquisition time for each image was about 80 ms and the two complete image acquisitions were acquired in one shot in 500 ms. This rapid velocimetry sequence gave a good representation of laminar pipe flow. It has also been used to examine extensional flow in a biaxial extension in which the transient extension takes about 3 s.

INTRODUCTION

In order to observe transient phenomena with NMR imaging, the use of rapid flow imaging techniques is necessary. Under these circumstances it is essential to have an observation time short relative to the time scale of the physical property to be measured. Transient phenomena include, for example, turbulent flow at high Reynolds number, flow and dispersion through porous media, and extensional deformation.

The best known techniques for rapid imaging are FLASH (*1*) and EPI (*2, 3*). Kose visualized turbulent motion in a circular pipe by using EPI (*4–6*). In those experiments, images were acquired in such a short time that the flow distribution did not change noticeably during the measurement time and they were able to produce a movie sequence of EPI images. He also used a one-shot velocity mapping employing a modified EPI sequence and applied it to turbulent flow to visualize vortices (*7*). Many groups have applied EPI techniques to observe transient dynamic processes (*8*) in porous media by "freezing the motion" (*9–11*). In the present article we demonstrate an application of echo planar imaging at microscopic resolution using single-shot phase encoding for flow via the pulsed gradient spin echo (PGSE) technique.

PGSE encoding has been previously used in such an application (*12*) but with multiple encoding steps and a resulting experiment time of many minutes. By contrast, our goal was to achieve a microscopic image, phase encoded for velocity, in a time of less than 1 s. We were motivated by a wish to image the velocity in a soft material under extension in a biaxial extension (i.e., uniaxial compression) cell. This device was first discussed by Callaghan and Gil in 1999 (*13*) in the context of spectroscopic investigation. However, the quantitative description of the transient motion under extensional deformation has not been yet reported. The deformation takes about 3 s as two plates squeeze the sample contained between them. In consequence the time resolution of the rapid imaging technique must be at least on the order of a few hundred milliseconds. We were particularly interested in measuring the flow image for velocity components transverse to the compression axis, in order to investigate the uniformity of the rate of strain field. In order to achieve a velocity image in such a short time we are unable to use either the "successive image frame movie" approach or the" full propoagator" approach, since there is insufficient time to acquire more than one or two images at maximum. We have sought to develop a method in which a velocity image can be acquired over a duration of less than 1 s.

We chose π-EPI in order to allow the investigation of soft matter including polymers possessing short T_2^*. The repetitive train of π RF-pulses also refocuses Zeeman dephasing due to diamagnetic susceptibility inhomogeneity in the compression cell. Our "one-shot" experiment consists of two successive $\pi-$EPI imaging sequences, one with and the other without a bipolar velocity encoding gradient as a prior filter. The resulting ratio ideally provides a phase shift in each pixel due to translational motion alone. Our experiment presents the added challenge of requiring microscopic spatial resolution in an extension cell for which the amplitude of compressive motion is around 3 mm. Our specific aim was to investigate whether deformation of a gel sample can be sufficiently described by pure extensional flow or whether additional shear effects have to be taken into account.

ONE SHOT *q*-ENCODED PEPI

The pulse sequence used in the present study is shown in Fig. 1 and is similar to the PEPI (π-EPI) sequence used by other groups (*14, 15*). Because of the incorporated Carr–Purcell train of π RF-pulses, the *k*-space trajectory jumps between the upper and the lower half of *k*-space, which necessitates a subsequent data sorting before Fourier transformation. The

1090-7807/01 $35.00

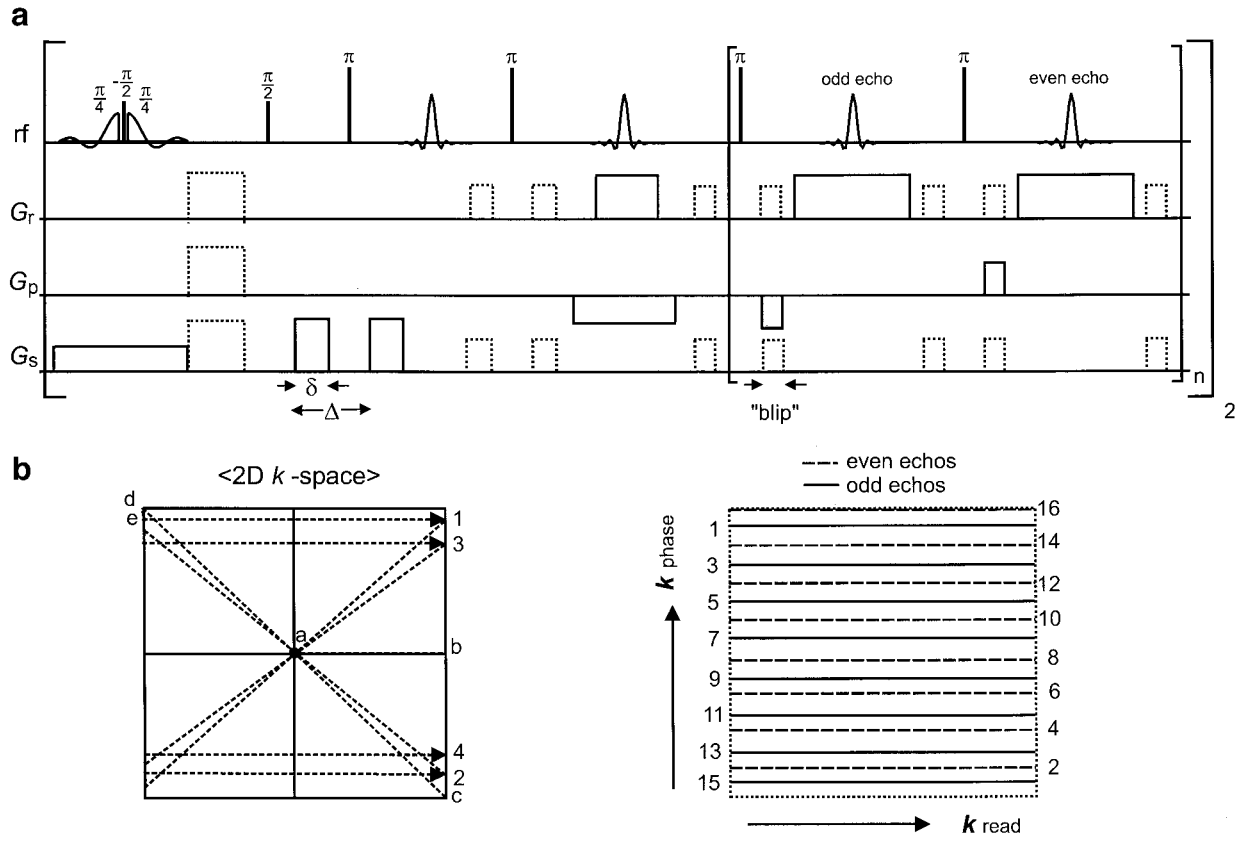

FIG. 1. (a) PEPI (π-EPI) pulse sequence with velocity encoding and pre-slice selection, as used in the present work. The dotted lines represents crusher gradients. During acquisitions crusher gradients are used in the read and the slice directions to avoid unwanted phase encoding effects. (b) Schematic diagram of raster used to acquire data in *k*-space. On the left are shown the trajectories, while on the right we see the interleaving of odd and even echo data.

basic raster is shown in Fig. 1b. The data are initially acquired at the borders of *k*-space, the low *k*-data being acquired at the middle of the echo train. The velocity encoding is realized by a spin-echo-based bipolar gradient pair as a filter preceding the PEPI imaging module.

One problem faced by any pulse sequence based on a CPMG train is the cumulative effect of imperfections in the RF excitation, imperfections which are only refocused in even echoes and not in the odd. This effect causes serious artifacts in the image. To minimize this problem, we used the idea of Manz *et al.* (*11*) of replacing the refocusing π-pulse by a composite sequence of three RF-pulses of $(\pi/2)_x$–$(\pi)_y$–$(\pi/2)_x$, giving a good spin-state inversion even for pulses with imperfect flip angle. The slice selection was realized by a self-refocusing selective storage sequence (*16*). A combination of a soft $(\pi/2)_x$ sinc pulse and a hard $(\pi/2)_{-x}$ pulse applied prior to the actual *q*-encoding PEPI sequence stores the signal from the desired slice as a longitudinal magnetization, while leaving undesired magnetization in the transverse plane, where it is subsequently dephased by crusher gradients applied in all three orthogonal directions. The advantage of this pre-slice-selective technique was that it permitted an arbitrarily short echo time in the subsequent EPI sequence, in our case, 2.4 ms. A conventional slice selection in which one replaces one of the initial $(\pi/2)_x$ or $(\pi)_y$ hard pulses by a soft sinc pulse in the presence of a gradient generally requires longer echo times. This is because of practical limitations associated with the gradient and RF power switching times which enter the duration of the first, and hence succeeding, echoes.

An inherent difficulty of PEPI is the differing amplitude and phase modulation and the relative *k*-space shift of even and odd numbered echoes. One reason is the RF imperfection effect referred to above. Another is the discrepancy between the precise area magnitude under the positive and negative *k*-space blips, resulting in a nonlinear *k*-space rastering after sorting the *k*-space data. These effects result in a ghost image which appears displaced along the phase encoding direction and shifted by one-half of the field of view. The problem can be minimized by using different *k*-space trajectories, by manual adjustment of gradient values to reduce this artifact, or by employing appropriate postprocessing techniques, for example, phase and amplitude correction of either even or odd numbered echoes. Any hardware solution is likely to be specific to the instrument used, while postprocessing makes inherent assumptions about the desired image phase, assumptions which can be dangerous when phase encoding is used to

obtain a velocity image. Given that, we handled with the problem in a simple manner by analyzing odd and even numbered echoes independently. Images from both sets were obtained and that with the better quality subsequently was chosen. If the total number of echoes remains fixed, as it generally must given echo time and T_2 limitations, the price paid for this approach will be a halving in the resolution along the phase direction. We employed a total of 32 echoes and 32 read-direction sampling points. The 16 phase-encoded data points for each of the odd and even echo sets were zero filled to 32 to produce 32×32 pixel images, in which the intrinsic resolution was 0.125×0.250 μm. For the chosen echo time of 2.4 ms, this resulted in a total acquisition time for one image of about 80 ms.

A second image, obtained under zero velocity-encoding gradient, is needed if one is to obtain the phase map necessary for velocimetry. The velocity map could be obtained by means of the image ratio method. Given that our gel sample had a T_1 relaxation time of around 300 ms, we were able to acquire the successive images in a single shot with a total acquisition time of about 500 ms.

ONE-SHOT PHASE-ENCODED VELOCIMETRY

The phase acquired by a spin isochromat arising from a fluid element with velocity ν in the presence of a standard PGSE encoding pair, as shown in Fig. 1, is given by

$$\phi = \gamma \delta G \nu \Delta. \qquad [1]$$

Each pixel of the image will acquire a local phase which ideally depends on the local fluid velocity component parallel to the encoding gradient direction. However, these phase shifts will coexist with additional phase artifacts, ϕ', associated with defects in the subsequent imaging sequence, artifacts which will be common to both the velocity-encoded and reference images. Furthermore the velocity-encoded and reference images may have differing amplitudes owing to incomplete relaxation recovery or to the effect of diffusive attenuation in the case of the image encoded with the PGSE pair.

In any given pixel, the ratio of the corresponding velocity-encoded and reference image amplitudes will be

$$\frac{S_G}{S_R} = \frac{|a_G| \exp(i\phi) \exp(i\phi')}{|a_R| \exp(i\phi')} = \frac{|a_G|}{|a_R|} [\cos \phi + i \sin \phi]. \qquad [2]$$

The value of ϕ may be obtained by taking a ratio of the imaginary and real parts of the signal and calculating the arctangent. Care must be exercised in unwrapping the phase where ϕ lies outside the range $-\pi$ to π.

APPLICATION OF EPI MICROSCOPY TO LAMINAR PIPE FLOW

All experiments reported here were carried out using a Bruker AMX300 NMR spectrometer equipped with a micro-imaging probehead and gradient system. The various flow and deformation cells used were homebuilt and fitted into the standard Bruker NMR probe within the widebore 7-T magnet. This probe permits sample dimensions of up to 25-mm radius.

The q-encoding PEPI sequence was tested using laminar pipe flow, for which a well-known parabolic velocity profile should be found. Water was pumped through a PTFE-tube of 2 mm inner diameter at a flow rate of 100 ml/h, giving an averaged velocity of 8.8 mm/s.

In order to clearly resolve the velocity profile of this pipe flow, a "field of flow" was chosen in which the maximum value of ϕ exceeded the arctangent range and was on the order of 2π. This led to a an observed wrapping of the parabolic phase dependence on radial position r, as expected. The PGSE velocity-encoding gradient had a duration of $\delta = 2$ ms and a amplitude of $G_\nu = 0.1$ T/m. An encoding time of $\Delta = 8$ ms between the bipolar gradient pair was chosen, resulting in a maximum phase value of $\phi = 8$ rad, considering the maximum velocity expected at 17.6 mm/s.

In Fig. 2a we show, for illustrative purposes, the cos ϕ distribution. It nicely demonstrates the effect of the known velocity profile and its resulting phase distribution where phase angles in excess of π are apparent. Figure 2c shows the effect of the phase wrapping ambiguity in the arctangent calculation in which ϕ lies outside the limits $-\pi$ to π. Figure 2b represents the two-dimensional velocity profile, calculated from the phase shift after correction of the phase wrapping by adding 2π at the phase jump. Note that a change of the sign of the velocity results in a phase shift of π. In our data such an effect is apparent with the zero velocity point corresponding to a phase of $-\pi$. We calculate the velocity amplitude by implementing a π phase shift. The velocity profile for Poiseuille flow in a pipe is expected to be parabolic and given by

$$\nu(r) = \nu_{\max} \left(1 - \left(\frac{r}{r_0}\right)^2\right), \qquad [3]$$

where r_0 is the inner wall radius.

Figures 2b and 2d show the experimental velocity profile (Eq. [3]) and the clear parabolic character demonstrates the quality of the PEPI velocimetry used in this work.

TRANSIENT FLOW IN A BIAXIAL EXTENSION CELL

The velocity-encoding $\pi-$EPI technique has also been applied to measure transient flow behavior in a biaxial extension cell in which a sample is squeezed between two approaching plates. The squeezing motion causes expansion in the two directions transverse to the squeeze axis and the velocity-

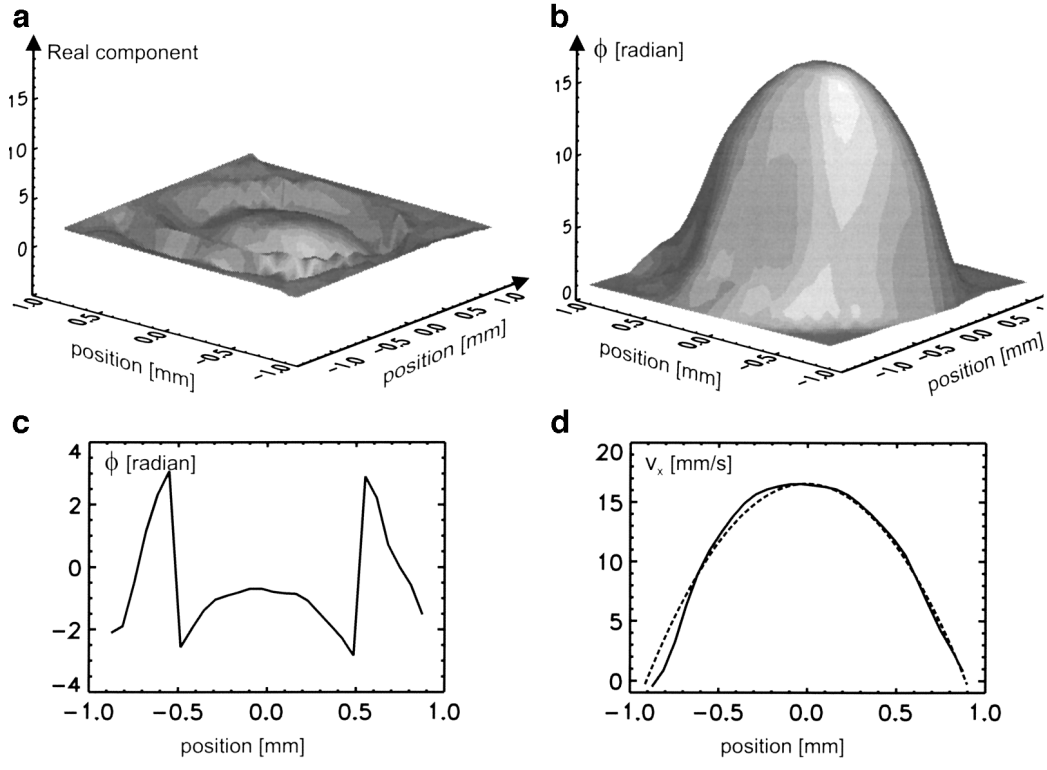

FIG. 2. Velocity mapping of laminar pipe flow using the q-encoding PEPI sequence. This results in a phase shift in each pixel proportional to the local velocity. (a) The real part of the data, in which a cos ϕ distribution is apparent. (b) Two-dimensional velocity profile obtained from the arctan analysis after correcting the phase wrapping. A paraboloid velocity distribution can be seen. (c) An exemplary one-dimensional phase distribution obtained from (a) with phase wrapping around $\phi = \pi$. (d) The straight line shows an exemplary one-dimensional velocity profile obtained from (b) after correcting the phase wrapping, giving a parabola with a maximum close to 17.6 mm/s, as expected. A theoretical parabola is fitted to this experimental velocity profile (dotted line).

encoding filter was set to encode for this transverse velocity. The sample compressed was a gel of cylindrical geometry with 3-mm height and 5-mm diameter. This gel was prepared from 2% κ-carrageenan (a polysaccharide extracted from seaweed) in a 0.1% $CuSO_4$ solution of distilled water. The biaxial extension cell used in the present work is illustrated in Fig. 3. The teflon plugs have a diameter of 16 mm and are initially separated by 3 mm before starting the squeezing process. The upper Teflon plug was attached by a shaft to a stepper motor and gearbox located at the top of the NMR magnet. The shaft rotates a screw which results in a downward movement with constant velocity. The rotation frequency was 0.11 Hz, with the upper Teflon plug moving downward with a velocity of 0.13 mm/s.

Figures 4a and 4c present EPI images before squeezing and during squeezing, respectively. As expected, these magnitude images show a fairly even distribution of spin density, although we do note that the sample mean position does not remain perfectly central during the squeezing process. The corresponding velocity maps derived from these images are presented in Figs. 4b and 4d. The velocity map before squeezing shows a reasonably homogeneous phase distribution, which is equivalent to ν = constant, whereas the image during squeezing contains a velocity gradient in the transverse direction.

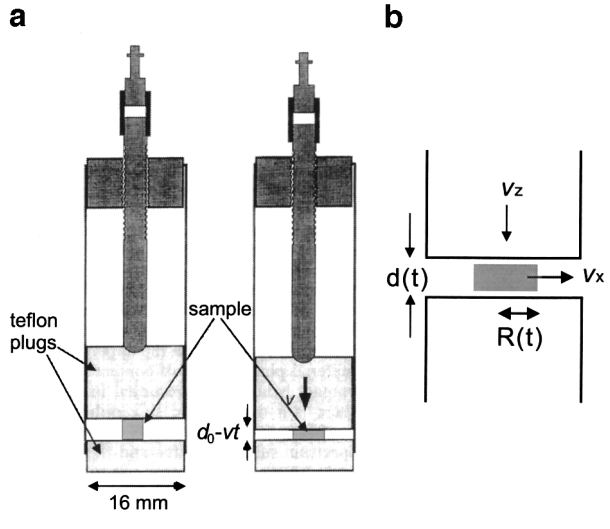

FIG. 3. Schematic representation of the biaxial extension cell. (a) The cell consists of a glass tube, where two Teflon plugs with 16-mm diameter are placed. The upper Teflon plug is connected to a shaft, which is in turn connected to a stepper motor. The rotating motion of the shaft is translated to a downward motion of the upper Teflon plug at constant velocity. The left figure represents the cell containing a sample before squeezing, while on the right the cell during squeezing of the sample is shown. (b) Definition of the coordinates x, z and the time-dependent radius, $R(t)$, and height, $d(t)$, of the sample, in which the local velocity components of a sample voxel are illustrated.

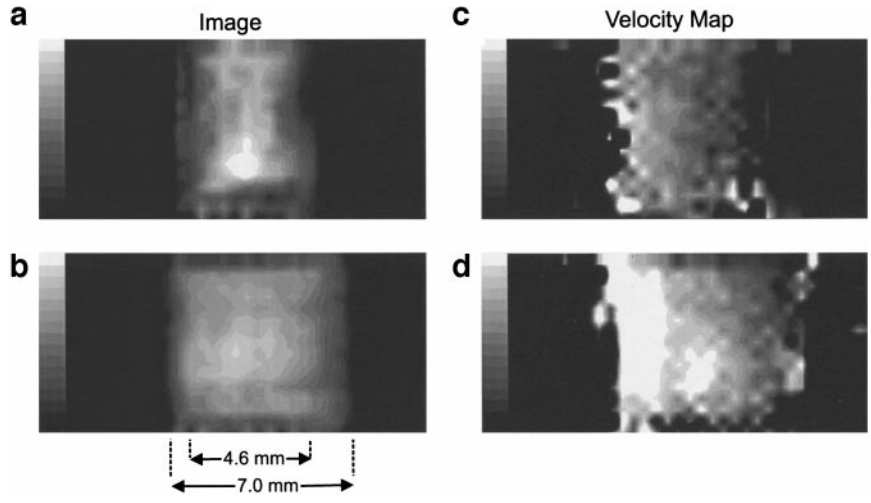

FIG. 4. Velocity mapping of extensional flow of gel sample in the biaxial extension cell. Motion encoding is for the (horizontal) direction transverse to the squeezing axis, i.e., along the direction of extension. (a) Magnitude (spin density) image of the gel sample before squeezing. (b) Magnitude image of the gel sample during squeezing. The field of view for both images was chosen to optimize vertical resolution in the squeezed sample. Consequently, in image (a) the vertical field of view is smaller than the sample extent and foldback effects are apparent. (c) Velocity map of the gel sample before squeezing. (d) Velocity map of the gel sample during squeezing. The scale units are in millimeters per second.

Because the volume of the sample is constant before and during squeezing,

$$R(t)^2 d(t) = \text{constant}. \qquad [4]$$

Thus

$$\frac{\partial R(t)}{\partial t} = \frac{R(t)}{2d(t)} \cdot \frac{\partial d(t)}{\partial t}. \qquad [5]$$

Replacing $\partial R(t)/\partial t = \nu_x$ and $\partial d(t)/\partial t = \nu_z$, we find

$$\nu_x = \frac{R(t)}{2d(t)} \cdot \nu_z. \qquad [6]$$

The longitudinal velocity is $\nu_z = 0.13$ mm/s and the height and radius of the sample before squeezing are $d(0) = 3$ mm and $R(0) = 2.3$ mm for $t = 0$, respectively. From the image in Fig. 4c, the averaged radius of the squeezed sample at the moment of image acquisition ($t = 1$ s) during extension can be extracted, which is $R(1) = 3.5$ mm. Using Eq. [4], the height of the sample $d(1)$ during extension and acquisition can be derived and Eq. [6] predicts that the transverse velocity at the outer radius of the sample will be $\nu_x = 0.18$ mm/s. (Note that the value of $d(1)$ which is measured is an average over the image acquisition time. Since it may be shown that $\nu_x \sim d(t)^{-3/2}$, the average value of ν_x which results over this acquisition time will be a little higher than predicted by a calculation using the average value of $d(t)$.)

In Fig. 5 some exemplary 1D profiles derived from the two-dimensional velocity map in Fig. 4d are presented. Although the data are somewhat noisy, they appear to show a constant velocity gradient along the transverse direction. The average outer radial velocity, ν_x, is coincident with the calculated value of about $\nu_x = 0.18$ mm/s. Furthermore, the image shows clearly that no shear effects occur during squeezing of the gel sample and that the deformation is purely extensional.

CONCLUSION

One-shot velocimetry using PEPI was for the first time applied to the study of transient deformation of a soft material in a biaxial extension cell. The whole sequence, containing two PEPI acquisitions, one with a prior velocity filter and the other as a reference, takes about 400 ms, allowing 80 ms per image. Given that the whole compression process takes about 3 s, such rapid velocimetry provides the only means of imaging the flow field in a sufficiently short observation time. The quality of this

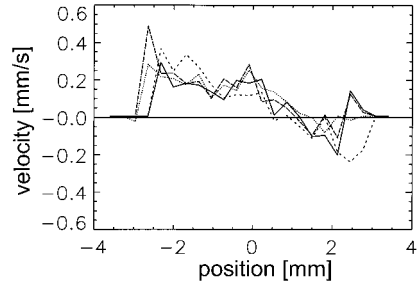

FIG. 5. Some exemplary one-dimensional velocity profiles obtained by selecting various cross-sections of Fig. 4d separated by 0.5 mm. The transverse velocity ν_x varies on average between −0.2 and 0.2 mm/s, as expected for purely extensional flow.

PEPI velocity imaging technique has been demonstrated using the well-known behavior of laminar pipe flow, resulting in a near-perfect parabolic velocity distribution. Furthermore, we have been able to obtain a two-dimensional velocity map of the transient extensional deformation using the one-shot PEPI sequence described above. This map quantitatively agrees with the expected velocity value and shows that, for the gel system used here, shear effects do not perturb the extensional flow during deformation in a biaxial extension cell.

ACKNOWLEDGMENTS

SH is a Ph.D. student of Professor Bernhard Blümich and this work was carried out during a 3-month visit by SH to the laboratory of PTC. We are grateful to Professor Blümich for providing the opportunity for this visit and funding support. PTC acknowledges funding support from the New Zealand Foundation for Research, Science, and Technology.

REFERENCES

1. M. Rokitta, U. Zimmermann, and A. Haase, *J. Magn. Reson.* **137,** 29 (1999).
2. P. Mansfield and I. L. Pykett, *J. Magn. Reson.* **29,** 355 (1978).
3. P. Mansfield, *J. Phys. C* **10,** L55 (1977).
4. K. Kose, *J. Phys. D* **23,** 981 (1990).
5. K. Kose, *J. Magn. Reson.* **96,** 596 (1992).
6. K. Kose, *J. Magn. Reson.* **98,** 599 (1992).
7. K. Kose, *Phys. Rev. A* **44(4)** 2495 (1991).
8. J. C. Gatenby and J. C. Gore, *J. Magn. Reson. A* **121,** 193 (1996).
9. D. N. Guilfoyle, P. Mansfield, and K. Packer, *J. Magn. Reson.* **97,** 342 (1992).
10. D. N. Guilfoyle and P. Mansfield, *J. Magn. Reson.* **119,** 151 (1996).
11. B. Manz, P. S. Chow, and L. F. Gladden, *J. Magn. Reson.* **136,** 226 (1999).
12. T. W. J. Scheenen, D. van Susschoten, and H. Van As, *J. Magn. Reson.* **142,** 207 (2000).
13. P. T. Callaghan and A. M. Gil, *Rheolo. Acta* **38,** 528 (1999).
14. D. N. Guilfoyle, P. Mansfield, and K. Packer, *J. Magn. Reson.* **97,** 342 (1992).
15. A. M. Peters, P. S. Robyr, R. W. Bowtell, and P. Mansfield, *Magn. Reson. Imaging* **14,** 875 (1996).
16. M. Kilfoil and P. T. Callaghan, *J. Magn. Reson.,* submitted.